To cite this version :

Epoxidized linseed oils based networks. Case of thermal degradation

Emmanuel Richaud [a], [*], Alain Guinault [a], Sarah Baiz [a], Fidèle Nizeyimana [b]

[a] Arts et Métiers ParisTech, CNRS, CNAM, PIMM UMR 8006, 151 bd de l'Hôpital, Paris, France
[b] ORANO TN, 1 rue des Hérons, 78180, Montigny-le-Bretonneux, France

A B S T R A C T

The thermal oxidation of networks based on epoxidized linseed oil cured with an anhydride hardener was studied in the 120−200 °C range by means of FTIR spectroscopy and gravimetry. Systems with 1-1 and 1−0.6 epoxy/anhydride stoichiometry were compared. The ageing tests monitored on thin films revealed that non-stoichiometric systems would be intrinsically more oxidizable than stoichiometric ones because of a higher concentration in reactive sites but stoichiometric system displays paradoxically higher levels of mass loss because those later originate from methyl cyclohexane hardener group. In the case of thick samples, the differences in oxygen diffusivity for both systems induce that oxidized layer would be slightly thicker in non-stoichiometric system than in stoichiometric ones would lead to lower in non-stoichiometric systems compared to stoichiometric ones.

1. Introduction

Some chemicals used for the synthesis of thermoset polymers are increasingly arousing concerns, as for example bisphenol A [1] and its release in environment after epoxy degradation [2], Diamino Diphenyl Methane (DDM) [3] used for epoxy curing, or styrene [4,5] used as reactive diluent in unsaturated polyesters. This makes compulsory to develop new thermoset matrices.

Biobased polymers coming from the biomass appear to be a promising alternative with several environmental advantages. Epoxidized oils obtained from the reaction of an oxidizing agent with the unsaturated fatty acids triglycerides can be envisaged as prepolymers. Diacids, some polyamide oligomers [6] or anhydrides are well soluble in epoxidized oils and reactive mixtures can be easily cured with the help of amine based catalysts [7,8] and curing times on the order of 1 h at temperature about 120 °C.

The resulting thermomechanical properties of those materials were already studied. They were shown to be comparable with several common organic matrices (with glassy elastic modulus and glass transition reaching respectively about 2 GPa and 100 °C [9]) which meets the expectation of applications.

However, their long term properties remain to be guaranteed. The oxidative stability of such compounds was already studied in the case of photochemical ageing [10] (at moderate temperature) allowing the knowledge of main photo-oxidation trackers (anhydrides, alkenes) and their consequences on macromolecular architecture (crosslinking predominating over chain scissions at short exposure times, those latter becoming progressively prominent at higher conversion rate). Apart in the case of very high temperature degradation (i.e. thermolysis [11]), the case of thermal ageing remains to be deeply investigated. We were thus interested in focusing on the thermal ageing in the 120−200 °C temperature range so as to have a better knowledge in:

- the stability of epoxidized linseed oils (ELO in the following) based matrices submitted to relatively high temperature thermal ageing,
- the Diffusion Limited Oxidation effects i.e. the effect of sample thickness on oxidation rate and the depth of degraded layer,
- the effect of anhydride hardener: it was already documented that the concentration of this latter permits to trigger the cost and initial thermomechanical properties, but less is known on the effect of non-stoichiometry on degradation mechanisms and long term properties to our knowledge.

2. Experimental

2.1. Materials

Epoxidized linseed oil (ELO) was kindly supplied by Arkema under the tradename Vikoflex 7190 with an oxirane content equal

to 9%. According to the fatty acids composition of linseed oil [8,12], it means that double bonds are almost 100% epoxidized. A general structure of ELO (aimed at representing the average of existing fatty acids triglycerides) and of other used reagents are given in Fig. 1.

Hexahydro-4-methylphthalic anhydride (MHHPA — $M = 168$ g mol^{-1} - CAS 19438-60-9) was used as hardener. It was supplied by Sigma Aldrich as a mixture of *cis* and *trans* (ref 149934).

2,4,6-Tris(dimethylaminomethyl)phenol (DMP30 - $M = 265$ g mol^{-1} - CAS 90-72-2) was used as cure catalyst. It was supplied by Sigma Aldrich (ref 45348 from Sigma Aldrich).

2.2. Cure conditions

Bulk samples were cured at 130 °C under vacuum during 6 h basing on DSC work previously published [13] with the following mass ratio: 20/19 for ELO + MHHPA 1-1 and 20/13 for ELO + MHHPA 1-0.6. Thin samples (typically 200 μm thick) were realized by curing a drop of reactive mixture under vacuum until it thickens. Just before gel point is reached (about 3 h), the mixture was cured using a laboratory Gibritte press overnight. After curing, great attention is paid to the residual concentration in oxirane ring. According to FTIR data (Fig. 2), it seems that oxirane (absorbing at 830 cm^{-1}) are almost totally consumed. However, we will consider the possibility of residual oxirane in some oxidation mechanisms.

Basing on the existing literature on epoxy-anhydride networks [14], it is thus expected that after curing:

- In ELO + MHHPA 1-1, all epoxide rings have reacted with anhydrides and crosslink nodes are methine groups in α-position of ester groups (Fig. 3a).
- In ELO + MHHPA 1-0.6, part epoxide rings have reacted with anhydrides and crosslink nodes are either methine groups in α-position of ester groups, or ether bridges (Fig. 3b).

The molar mass of repetitive constitutive units are given in Table 1 together with the number and the concentration in CH$_2$ being considered here as an "internal standard" for curves normalization and the concentration some of the main reactive sites.

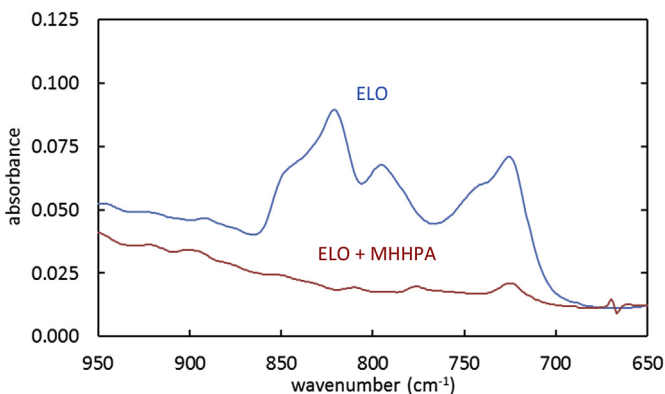## 2.3. Exposure conditions

Ageing was performed:

Fig. 2. FTIR analysis of unreacted ELO and cured ELO + MHHPA 1-0.6.

- In ventilated ovens (AP60 supplied by SCS) at 120, 160 and 200 °C,
- In autoclaves (TOP industries) at 160 °C under 1.0 MPa of pure oxygen.

Some complementary ageing tests were directly performed in situ in TGA cell as described below. Geometries of samples studied in each case will be detailed in sections below.

2.4. Characterization

2.4.1. Fourier transform InfraRed spectroscopy

FTIR in transmission mode were performed on free standing 20 μm films using a Frontier 100 apparatus (PerkinElmer) by averaging 16 scans with a 4 cm^{-1} resolution.

2.4.2. Thermogravimetric analysis

Thermogravimetric analysis were performed using a Q50 apparatus (TA Instruments) driven by QSeries Explorer software. Thin samples (about 50–75 μm thin) were placed in platinum pan and subjected to isothermal exposure at 200 °C under 100% O$_2$ or 100% N$_2$ atmosphere supplied by a 50 ml min^{-1} gas flow. Results were exploited using TA Analysis software.

2.4.3. Volatile analysis

The volatiles evolved during a 60 min exposure under 1 bar O$_2$ or 1 bar N$_2$ at 200 °C were concentrated in a sealed vial. They were analyzed in GC MS with a headspace injector.
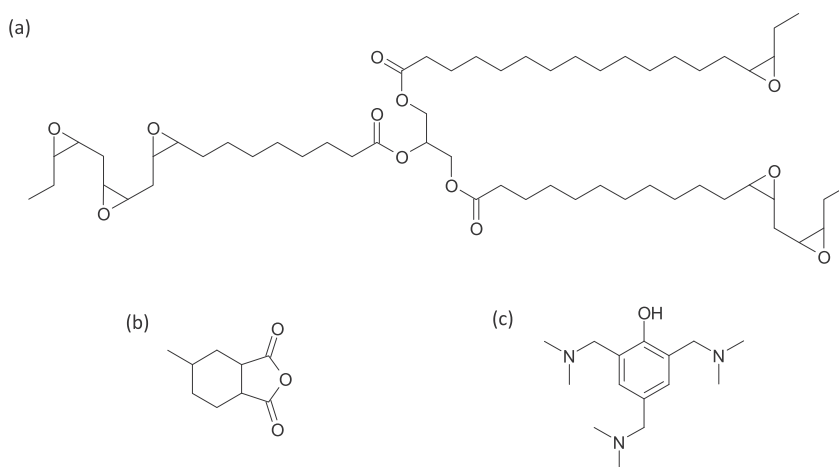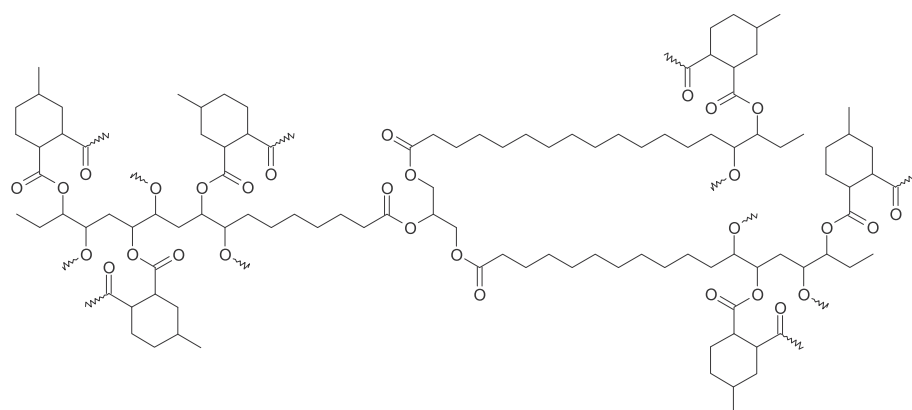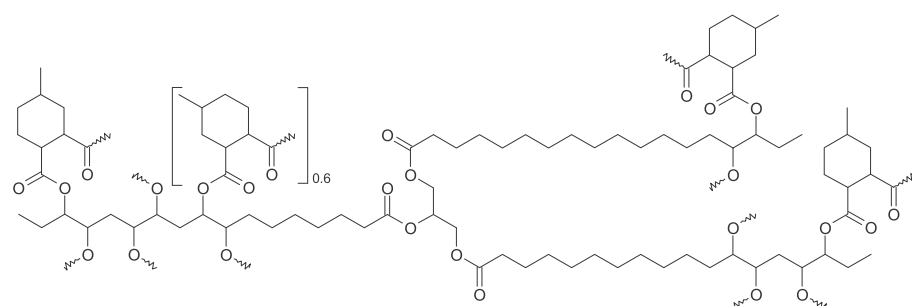

Fig. 1. Typical structure of ELO (a), MHHPA (b) and DMP30 (c).

(a)

(b)

Fig. 3. Proposed repetitive constitutive unit of ELO + MHHPA 1-1 (a) and ELO + MHHPA 1-0.6 (b) (NB: the 0.6 subscript accounts for the stoichiometry and ether and ester crosslink bridges are randomly located).

Table 1
Main characteristics of networks (the concentrations of reactive sites are given in mol kg^{-1}).

reactive group	ELO + MHHPA 1-1 ($M_u = 1982$ g mol^{-1})	ELO + MHHPA 1−0.6 ($M_u = 1578.8$ g mol^{-1})	product
ester	7.6	6.5	→ anhydride
ether	0	3.0	→ anhydride
ether ether	0	0.8	→ biacetyl ?
MHHPA	0.5	0.4	→ volatiles
>CH$_2$	28.3	30.9	

The signals from the mass spectra range of 10−200 (m/z) are identified as the major contributors from the specific evolved gases and volatiles, according to the database of National Institute of Standards and Technology.

2.4.4. Optical microscopy

After thermal ageing and prior to observations, thick samples were polished so as to obtain a smooth and mirror like finish and observed using a Zeiss Axio Imager A2M optical microscope in reflection mode (dark field episcopy). Data were exploited by Axiovision SE64 rel 9.4.1 software.

2.4.5. Micro indentation

A microindenter allows the measurement of the hardness of a material on a microscopic scale, through its resistance to permanent deformation or damage [15]. After impressing the indenter into the material at loads from a few grams to 1 kg, a hardness value can be calculated from automatic measurements of the impressed area and the maximum force, while force and penetration measurements during the elastic portion of the unloading can be used to estimate local values of the elastic modulus within the sample [16].

The indentations were here carried out in the commonly used Vickers hardness scale using a diamond square-based pyramid

indenter. A series of hardness impressions were made along a line, at a distance of 200 μm from one of the two outer surfaces, reaching the core of the sample with an increasing step size, in order to systematically measure the hardness variation within the samples, and detect the possible presence of a superficial oxidized layer through its effects on the material's local hardness and/or elastic modulus. Prior to testing, the samples were mounted and polished to provide smooth, parallel surfaces. A CSM Instruments (Anton PAAR) MHT microindentation platform was used. Surface detection force was 20 mN and indentation force was 150 mN. Loading and unloading were carried out at 5 mN s^{-1}, and stabilization was set at 10 s. HV_{IT} and E_{IT} values were plotted as a function of the distance from one of the outer surfaces.

The Anton Paar TriTec Indentation software (version 7) of the MHT CSM microindentation device calculates the Vickers microhardness HV_{IT} using the following formula:

$$HV_{IT} = \frac{F_{max}}{10.85 \times A_{max}} \quad (1)$$

F_{max} and A_{max} being respectively the maximum test force (here 150 mN) and the contact area at maximum test force, obtained from a calibration curve. 10.850 is the geometrical correction factor for a Vickers shaped indenter used in this software.

The indentation (elastic) modulus E_{IT} was here calculated from the following equation:

$$E_{IT} = E^* \times (1 - \upsilon_S)^2 \quad (2)$$

υ_S is the estimated sample Poisson's ratio (here υ_S is supposed here to be constant with ageing time and equal to 0.4), and E^* is defined by the following equation:

$$\frac{1}{E^*} = \frac{1}{E_r} - \frac{1 - \upsilon_i^2}{E_i} \quad (3)$$

where E_i and υ_i are respectively the elastic modulus and the Poisson's ratio of the indenter (respectively equal to 1141 GPa and 0.07), and E_r is calculated from the following equation:

$$E_r = \frac{\sqrt{\pi} \cdot \frac{dF}{dh}}{2\beta\sqrt{A_{max}}} \quad (4)$$

β is a geometrical factor equal to 1.012 for a square-based indenter and $\frac{dF}{dh}$ is calculated over 40%–98% of F_{max} on the unloading load-displacement curve, using the Oliver & Pharr power law fit, as this portion of the unloading curve may not be linear [17].

2.4.6. Permeation

As received 20 μm thin films maintained in a flexible aluminum mask (with an accessible surface ca 5 cm^2) were placed between the two compartments of a Systech 8001 permeameter. The cell and the sample were completely purged during one week in order to avoid oxygen diffusivity underestimation due to residual oxygen present in the polymer bulk. Purge was performed at room temperature to avoid in situ oxidation. Pure oxygen (99.9%) was then introduced into the upper half of the chamber while an oxygen-free carrier gas flowed through the lower half. A coulometric sensor monitored the oxygen flow through the sample induced by oxygen pressure difference. The time lag τ expresses the time which is necessary for oxygen to go across the sample. The analytical solution of Fick's law in a case of an infinite plate of thickness L with penetrant at a C_s concentration on one edge and 0 at the other allows to determine the diffusion coefficient of oxygen by the equation [18,19]:

$$\tau = L^2 / 6D_{O2} \quad (5)$$

Measurements were performed at 23, 40 and 50°C at 0% RH. They are given in Fig. 4. Given the very long time needed for each single measurement (about 3–4 weeks), all measures were performed only once.

Those values call for the following comments:

- They obey Arrhenius law consistently with other thermosets tested in their glassy state
- The measured values are obviously higher for diffusivity and permeability than in other thermosets (see "Appendix 1"). This is however well in agreement with the depth of degraded layers which are greater than in other thermosets.
- The value for ELO + MHHPA 1-0.6 seems even higher than ELO + MHHPA 1-1. This will be discussed later in the discussion section (for discussing the Diffusion Limited Oxidation aspects).

3. Results

3.1. Chemical changes

Fig. 5 displays results for thermal ageing followed by FTIR:

- FTIR in the carbonyl region are given in Fig. 5a and b respectively for ELO + MHHPA 1-1 and ELO + MHHPA 1-0.6
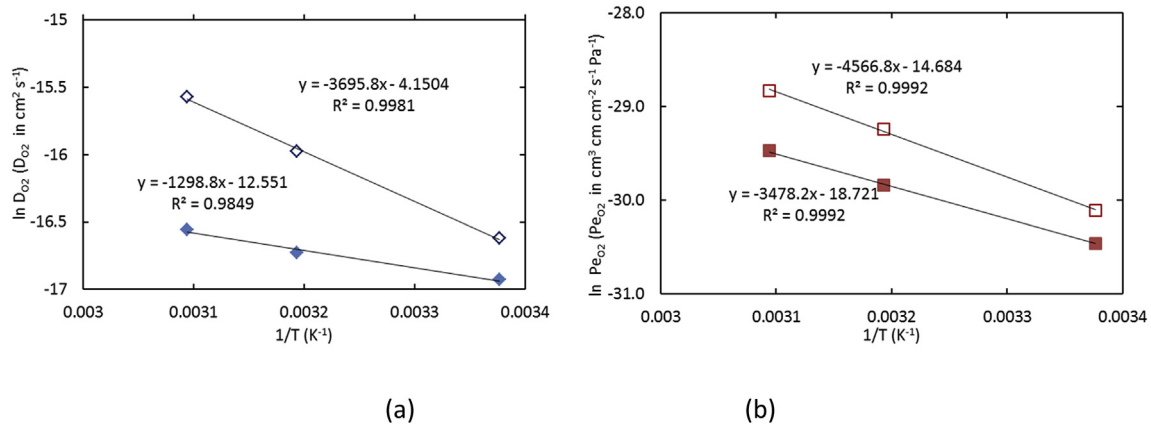

(a)   (b)

Fig. 4. Diffusivity (◆: ELO + MHHPA 1-1, ◇: ELO + MHHPA 1-0.6) and permeability (■: ELO + MHHPA 1-1, □: ELO + MHHPA 1−0.6) of virgin networks.
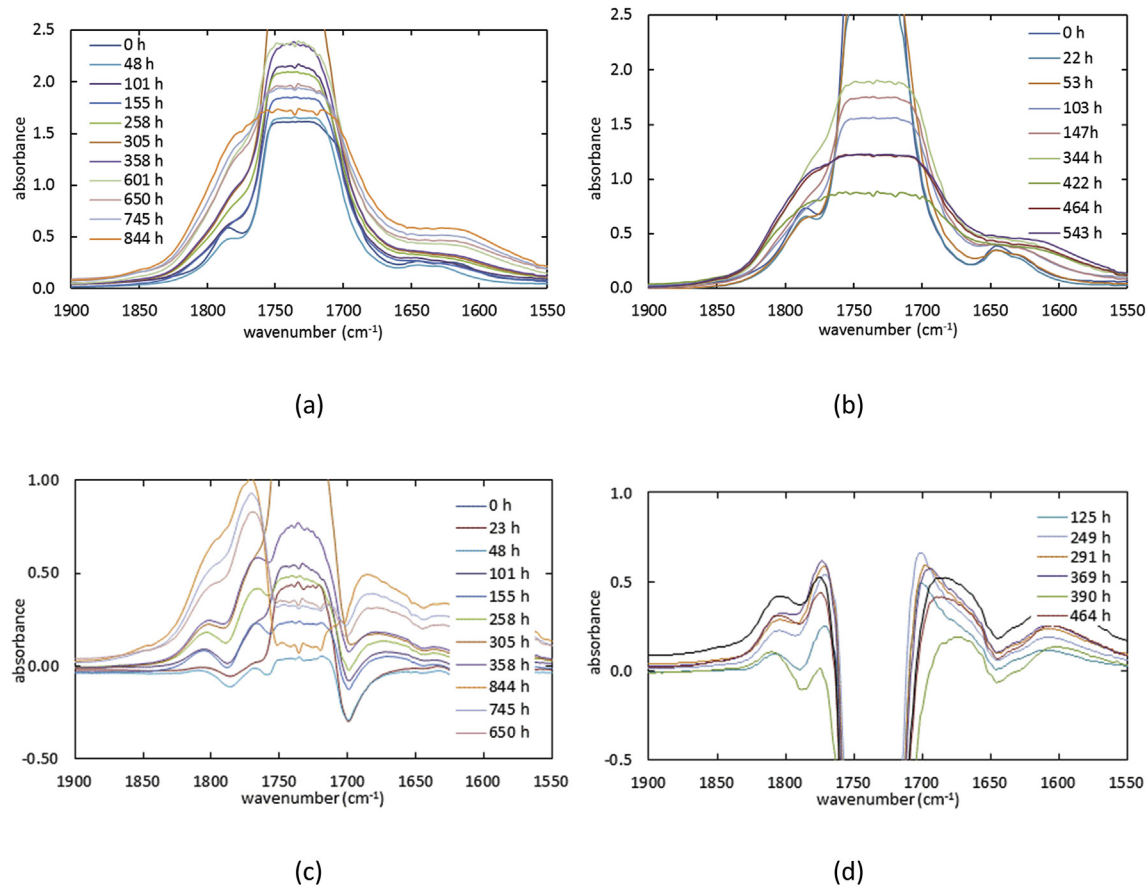
Fig. 5. FTIR spectra of ELO + MHHPA 1-1 (a) and ELO + MHHPA 1-0.6 (b) and subtraction to the spectra of unaged material for ELO + MHHPA 1-1 (c) and ELO + MHHPA 1-0.6 (d).

- The subtraction of spectra of aged materials to the unaged one are given in Fig. 5c and d respectively for ELO + MHHPA 1-1 and ELO + MHHPA 1-0.6

They call for the following comments:

- The carbonyl spectra clearly display a strong broadening in both cases.
- The ester groups are consumed and disappear, but this seems more pronounced for the ELO + MHHPA 1-0.6. In other words, the height of oxidation signals (see later) can be underestimated in this second case.
- The subtraction reveals, for each exposure conditions and each stoichiometry, the presence of a doublet at 1805 and 1770 cm^{-1} ascribed to the asymmetric and symmetric stretching of anhydrides functions [20−22], the formation of which will be justified in the "Discussion" section.
- The subtraction shows another maxima on the right wing of carbonyl peak, located at around 1680 cm^{-1}. The comparison of Fig. 5c and d suggests (and it will be more precisely quantified in the following) that this signal is more pronounced for ELO + MHHPA 1-0.6 than ELO + MHHPA 1-1 system. It seems also that this peak is more visible for « soft » ageing conditions (120 and 160 °C under air) than severe ones (160 °C under 1.0 MPa O$_2$ and 200 °C under air).

In order to make a quantitative comparison of both systems, absorbances were measured from susbtracted spectra. Anhydride concentration was assessed from Beer Lambert:

$$[Anh] = \frac{\varepsilon_{CH_2}}{\varepsilon_{Anh}} \times [CH_2] \times \frac{A_{1805}}{A_{1457}} \tag{6}$$

where [Anh] and [CH$_2$] are respectively the concentrations in anhydrides and methylenes, ε_{Anh} and ε_{CH2} their molar absorptivity and A_{1805} and A_{1457} the corresponding absorbances.

The kinetics of oxidation were thus estimated by plotting the changes of the normalized absorbance of anhydride estimated by the quantity $A_{1805}/A_{1457} \times [CH_2]$ where CH$_2$ is given in Table 1. The kinetic curves displayed in Fig. 6 indicate that ELO + MHHPA 1-0.6
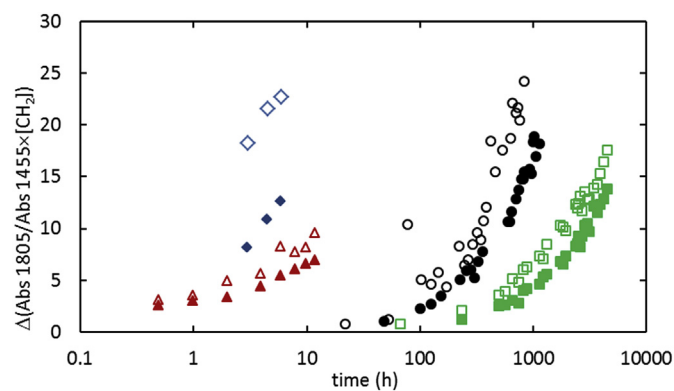

Fig. 6. Kinetic curves for anhydride formation (normalized to 1455 cm^{-1} as internal standard) for ageing under 1.0 MPa O$_2$ at 160 °C (◆,◇), and under air at 200 (▲,△), 160 (●,○) and 120 °C (■,□). Open symbols correspond to ELO + MHHPA 1-0.6 and closed symbols to ELO + MHHPA 1-1.
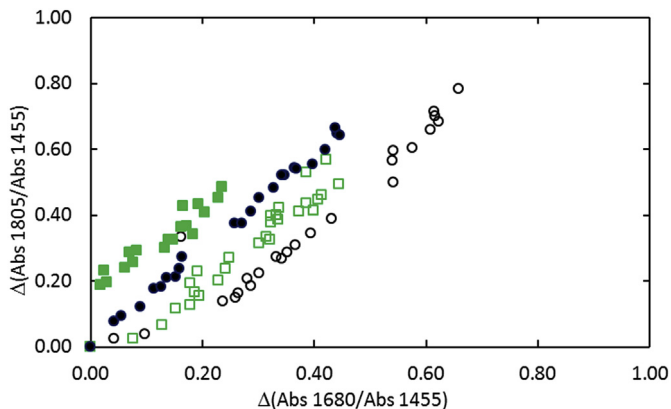
Fig. 7. Plot of anhydride formation versus $1680 \, \text{cm}^{-1}$ (normalized to $1455 \, \text{cm}^{-1}$ as "internal standard") for ageing under air at 160 (○,●) and 120 °C (■,□). Open symbols correspond to ELO + MHHPA 1−0.6 and closed symbols to ELO + MHHPA 1-1.

are more sensitive than ELO + MHHPA 1-1 to oxidation in terms of formation of anhydrides.

About the $1680 \, \text{cm}^{-1}$ absorbance, we were interested in characterizing its occurrence by plotting the changes in (normalized) absorbance for anhydrides versus the changes in this absorption (Fig. 7). It unambiguously shows that the formation of products absorbing at $1680 \, \text{cm}^{-1}$ is favored by ELO excess. The possible nature of this product will be proposed in the 'Discussion' section.
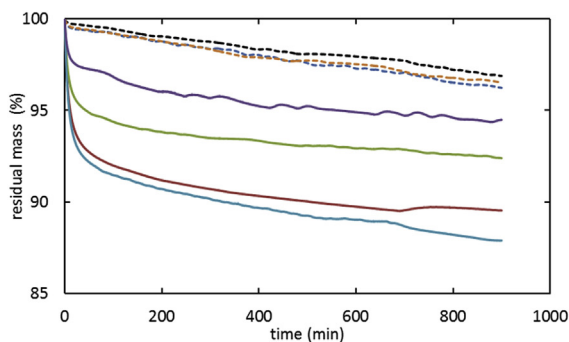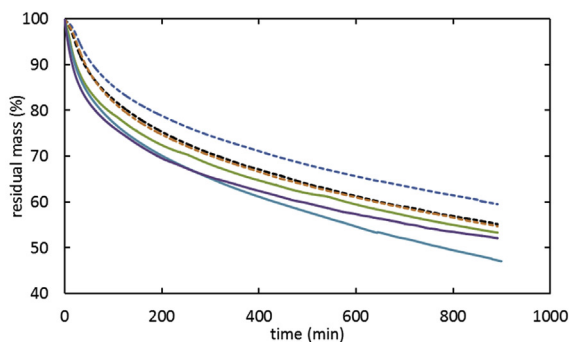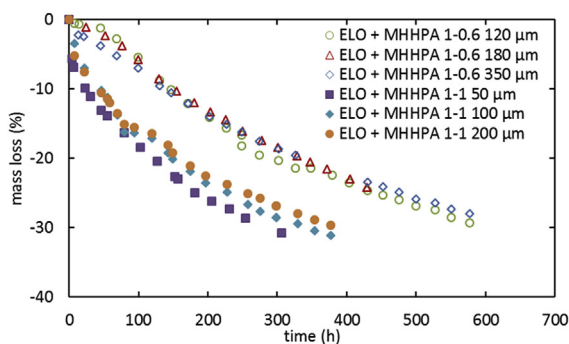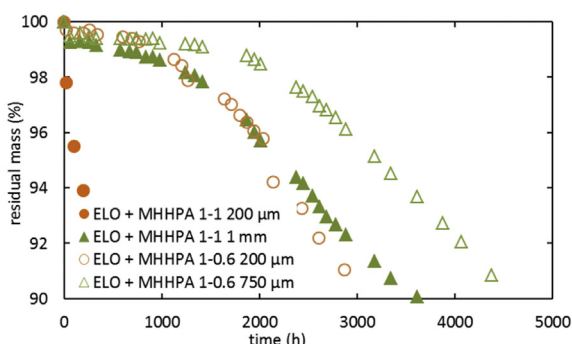
3.2. Gravimetric study

It is well established that the oxidation results in the release of volatile compounds expected to induce further shrinkage and cracking [23]. The thermal stability was hence first investigated by performing tests under inert atmosphere at 200 °C for samples with thickness ranging from 50 to 75 μm (Fig. 8a). Despite some scattering linked to sample thickness (in particular for ELO + MHHPA 1-1), it seems clear that in such conditions ELO + MHHPA 1-0.6 are more stable than ELO + MHHPA 1-1. The same is observed under 100% O_2 (Fig. 8b).

The same kind of experiments were conducted at lower temperatures (160 °C) under air for samples having a thickness below the threshold above which oxidation is controlled by oxygen diffusion, as it will be detailed in the next section. For summarizing the results presented in Fig. 9a:

- gravimetric curves for samples with a thickness ranging from 50 to 200 μm (for ELO + MHHPA 1-1) and 120−350 μm (for ELO + MHHPA 1-0.6) almost overlap (within the range of experimental error). In other words, the observed behavior only depends on the intrinsic reactivity of the system.

- it seems that ELO + MHHPA 1-0.6 display a short induction period (almost 50 h at 160 °C) contrarily to ELO + MHHPA 1-1 where mass loss starts almost instantaneously. This even more visible for sample aged at 120 °C where for example, the induction period for a ELO + MHHPA 1 mm thick is about 2000 h versus about 1500 h for a thinner ELO + MHHPA 1-0.6 (750 μm).

The mass loss actually is the sum of two contributions:

(a)

(b)

Fig. 8. Gravimetric curves for ELO + MHHPA 1-1 (full line) and ELO + MHHPA 1-0.6 (dashed lines) aged at 200 °C under N_2 (a) and under O_2 (b). (NB: Tests were repeated several times which correspond to several colored curves).

(a)

(b)

Fig. 9. Gravimetric curves for ELO + MHHPA 1-1 and ELO + MHHPA 1-0.6 aged at 160 °C (a) and 120°c (b) under air.
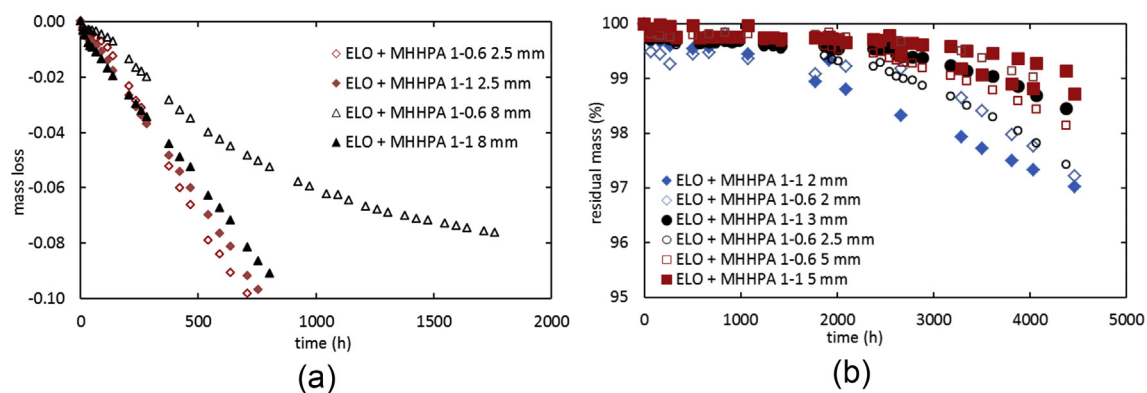
Fig. 10. Gravimetric curves for ELO + MHHPA 1-1 and ELO + MHHPA 1-0.6 aged at 160 °C (a) and 120°c (b) under air.

- The thermolytic effects being in principle observable irrespectively of the sample thickness,
- The thermo-oxidative ones, occurring only at the sample surface.

To highlight the possible differences associated to thickness in oxidized layer (between ELO + MHHPA 1-1 and 1-0.6), some thick samples (>2 mm) were aged and the mass loss are compared in Fig. 10a and b. For each kind of samples and both investigated temperatures, the kinetics of mass loss are slower with decreasing thickness. However, the differences between ELO + MHHPA 1-1 and 1-0.6 become almost negligible for thicker samples. For example at 120 °C, the 5 mm thick samples lose almost 2% after 5000 h irrespectively of the stoichiometric ratio. This last result will be interpreted in terms of Diffusion Limited Oxidation effects in the next section.

The main volatiles were detected by Gas Phase Chromatography coupled with mass spectrometry. Three samples were investigated because of their relatively high level of mass loss (Fig. 8):

- ELO + MHHPA 1-0.6 aged 60 min at 200 °C under 1b O_2
- ELO + MHHPA 1-1 aged 60 min at 200 °C under 1b O_2
- ELO + MHHPA 1-1 aged 60 min at 200 °C under 1b N_2

The main detected volatiles compounds are given in Table 2. It seems that they are associated to the methyl cyclohexane group belonging to the anhydride hardener (or its oxidation by products as for example 3 or 4 methyl cyclohexanone). At this stage, this result seems paradoxical since FTIR results suggest that ELO + MHHPA 1-1 would give a lower quantity of oxidation products but a higher level of mass loss.

Table 2
Main volatiles detected by GC-MS.

|	name	CAS	%	total area (u.a.)
ELO + MHHPA 1-1 100% N_2 200 °C 60 min	dimethylformamide	68-12-2	3.3%	
	3-methylcyclohexanone	591-24-2	2.1%	
	4-methylcyclohexanone	589-92-4	1.6%	4.95E+07
	2-methyl-1-octen-3-yne	17603-76-8	2.0%	
	4-methylcyclohexene	591-47-9	89.2%	
ELO + MHHPA 1-1 100% O_2 200 °C 60 min	4-methylcyclohexene	591-47-9	8.5%	
	hexanal	66-25-1	2.0%	
	N,N-dimethylformamide	68-12-2	2.3%	
	3-methylcyclopentanone	1757-42-2	2.4%	
	3-methylcyclohexanone	591-24-2	16.3%	
	4-methylcyclohexanone	589-92-4	13.2%	
	nonanal	124-19-6	3.1%	6.30E+07
	5-ethyl-2(5H)-furanone	2407-43-4	1.7%	
	2-methyl-1-octen-3-yne	17603-76-8	2.8%	
	4-methylcyclohexene	591-47-9	35.8%	
	1,4-cyclohexanedimethanamine	2549-93-1	1.0%	
	6-methyl-bicyclo[4,2,0]octane-7-one		1.2%	
ELO + MHHPA 1−0.6 100% O_2 200 °C 60 min	4-methylcyclohexene	591-47-9	9.1%	
	hexanal	66-25-1	6.2%	
	N,N-dimethylformamide	68-12-2	1.9%	
	3-methylcyclopentanone	1757-42-2	3.4%	
	heptanal	111-71-7	1.5%	
	2-pentylfuran	3777-69-3	2.6%	
	3-methylcyclohexanone	591-24-2	22.6%	
	4-methylcyclohexanone	589-92-4	18.4%	7.32E+07
	n-octylformate	112-32-3	3.0%	
	nonanal	124-19-6	7.6%	
	2-decanone	693-54-9	1.5%	
	4,4,6-Trimethyl-cyclohex-2-en-1-ol		1.0%	
	2-methyl-1-octen-3-yne	17603-76-8	1.4%	
	4-methylcyclohexene	591-47-9	8.7%	
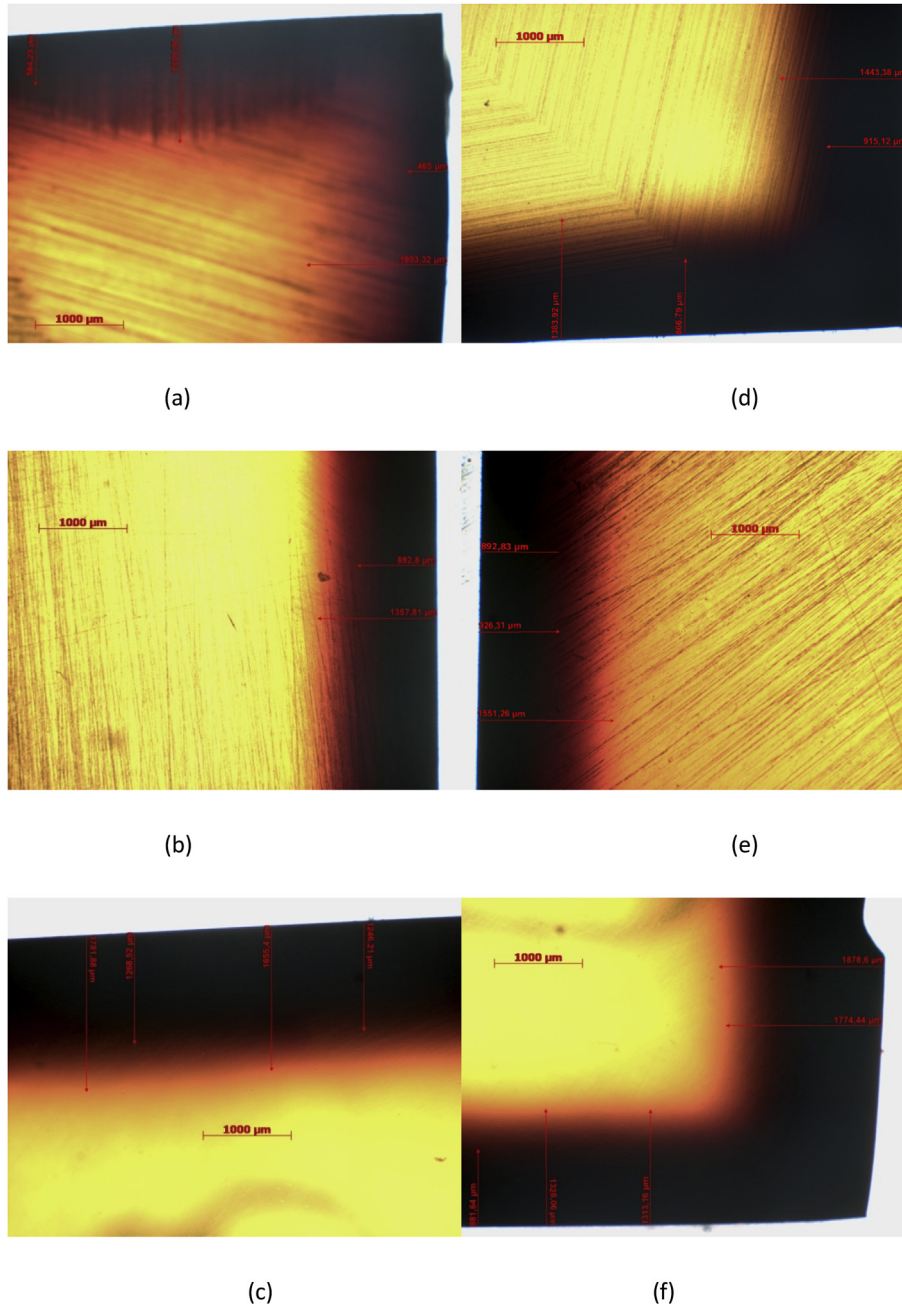
Fig. 11. Microscopic observations of oxidized Layers for ELO MHHPA 1-0.6 aged at 160 °C during 4 weeks (a), 12 weeks (b), 16 weeks (c), and ELO MHHPA 1-1 aged at 160 °C during 4 weeks (a), 12 weeks (e) and 16 weeks (f). NB: the scale bar corresponds to 1 mm.

3.3. Oxidation of bulk materials

In the case of bulky materials with a thickness around 1 cm, the diffusion reaction coupling of oxygen leads to the appearance of an oxidized layer. This latter can be easily observed by optical microscopy (Fig. 11) where the chemical changes (illustrated by FTIR spectra) result in UV absorbing structures responsible for dark edges and progressive fading of color change in the deepest layers. We arbitrarily considered the total colored zone as the oxidized layer [24,25]. The thickness of degraded layer reaches relatively fast a constant value [26] (only depending of the temperature and external oxygen concentration). Interestingly, it seems that its value is almost the same for both the stoichiometric and non-stoichiometric materials and roughly close to 1500 μm.

It has been shown that a chemical change, from non-oxidized to oxidized state, translates in a change in the local mechanical response of the oxidized [26,27]. Based on this phenomenon, it is acceptable to assume that TOL estimations based on a chemical criteria - i.e. oxidation leading to a color change visible by optical microscopy should be very close to TOL estimations based on a mechanical criteria, i.e. thickness of the layer having different hardness than that of the non-oxidized material bulk. TOL estimation based on local material hardness was obtained by micro-indentation measurements.

Firstly, it must be emphasized that indentation moduli (related to elasticity) and hardness (related to plasticity) display the same trends (i.e. an increase from bulk to surface and during oxidation). This behavior is consistent with previous observations on other

epoxy thermosets [25], indentation measurements revealed an increase in the elastic moduli when approaching to the surface, i.e. in the oxidized layer. Two explanations can be proposed for the increase of modulus with oxidation:

- An increase in cohesive energy due to the conversion of moderately polar esters into anhydrides and carboxylic acids. A simplified explanation is given in Appendix 2.
- A disappearance of the sub glassy transition due to the degradation of some groups associated to sub glassy relaxation. This sub glassy transition might involve the diester segments [28] consistently with the mechanisms proposed in the discussion section but this remains to be investigated using DMA which goes out of the scope of the present paper.

Despite the absence of a definitive explanation, it is however clear that the thickness of oxidized layer (TOL in the following) is lower for ELO + MHHPA 1-1 (about 1500−2000 μm) than ELO + MHHPA 1-0.6 (2000−2500 μm). Such values are higher than in other common thermosets (for example 600 μm in polyesters at 160 °C [24] and almost 300 μm in aromatic epoxies [24] which is consistent with the higher permeability values in ELO + MHHPA (see Appendix 1).

4. Discussion

The main aims of this section are to explain:

- The nature of the physico-chemical changes observed during ELO + MHHPA oxidation,
- The role of stoichiometry on oxidation kinetics, mass loss and thickness of degraded layers.

4.1. On the formation of stable products

Identically to unsaturated polyesters and vinylester networks [24,29], the formation of anhydrides must result from the oxidation of C-H in α position of ester groups. According to the structure of ELO + MHHPA 1-1 and ELO + MHHPA 1-0.6 networks, there are at least two reactive sites likely to give anhydrides by a "direct" in chain radical mechanism:

- The methine groups in α-position of ester functions belonging to hardener,
- The methylene groups hold by glyceryls.

The corresponding possible mechanisms are given in Scheme 1. However, if anhydrides were formed only from the oxidation of

(a)

(b)
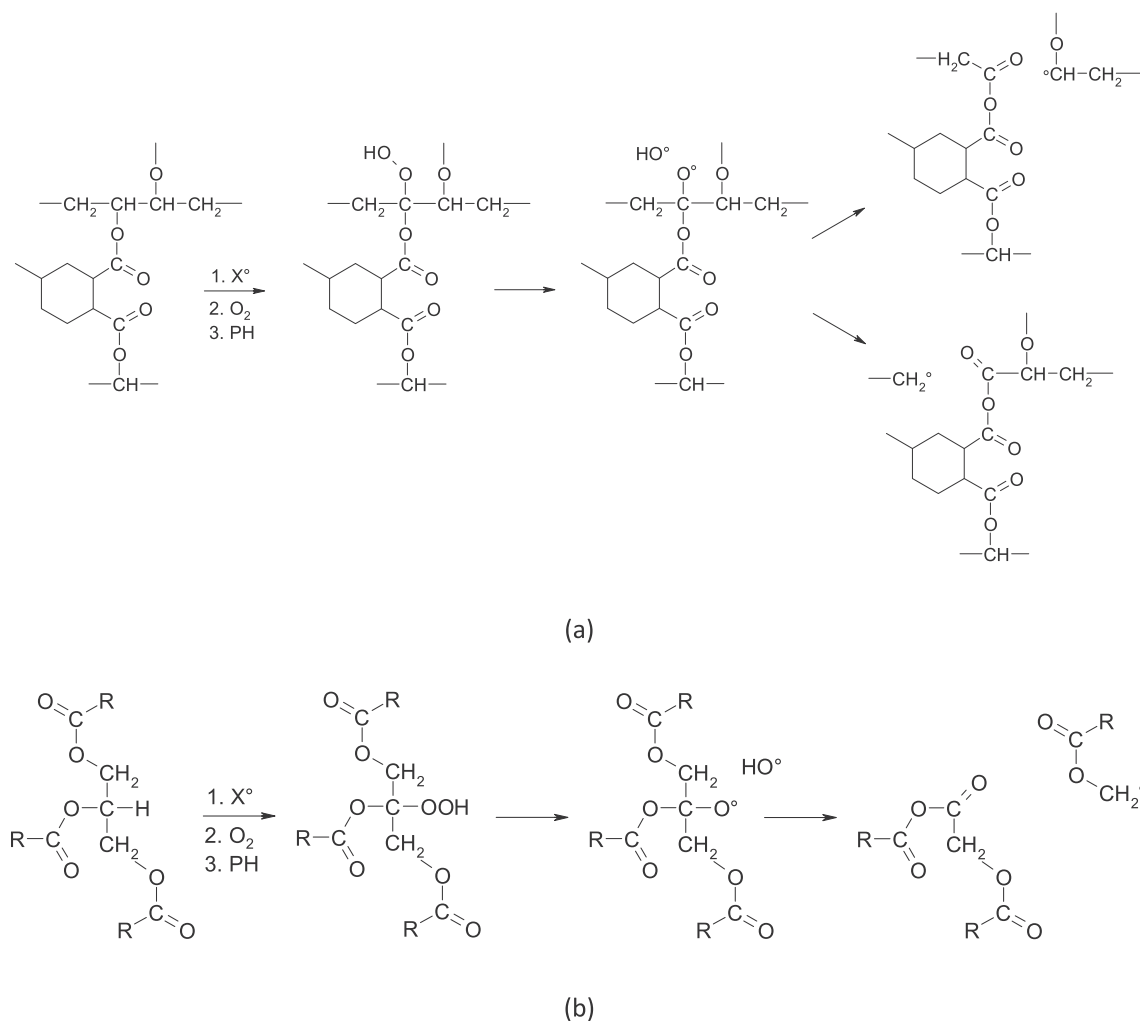
Scheme 1. Formation of anhydrides in ELO + MHHPA 1-1 and ELO + MHHPA 1-0.6 from C-H at vicinity of hardener groups (a) and CH$_2$ hold by glyceryls (b).

(a)

(b)
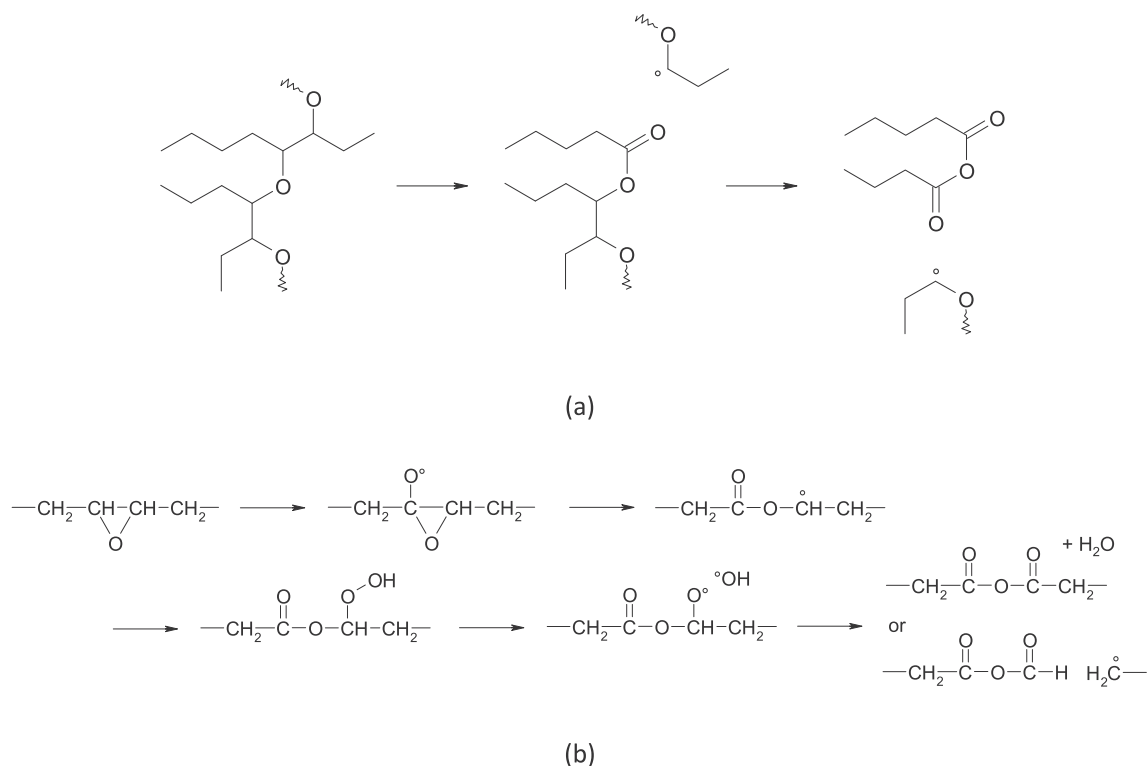
Scheme 2. Possible mechanisms of anhydrides formation in ELO + MHHPA 1-0.6 from C-H at vicinity of ether bridges (a) and residual unreacted epoxides (b).

CH in α position of esters groups, ELO + MHHPA 1-1 would be more oxidizable than ELO + MHHPA 1-0.6 since the concentrations of CH_α are respectively equal to 7.6 and 6.5 mol kg^{-1} (Table 1). It means that other kinds of CH participate to oxidation to give anhydrides in the same timescale. Two other mechanisms presented in Scheme 2 can be proposed:

- The oxidation of CH at vicinity of ether bridges
- The oxidation of residual oxirane rings

In the constitutive unit of ELO + MHHPA 1-0.6 (Fig. 3b), the number of such CH is equal to 4.8 i.e. their concentration is close to 3 mol kg^{-1} (Table 1). In other words, the concentration of such sites cannot be neglected compared to the concentration of CH in α position of ester groups (Table 1). The orders of magnitude of Bond Dissociation Energies for corresponding bonds are known:

- BDE $(CH_{\alpha\text{-ester}}) \sim 400$ kJ mol^{-1} (basing on estimations in ethyl acetate) [30,31].
- BDE $(CH_{\alpha\text{-ether}}) \sim 392$ kJ mol^{-1} [32] in THF
- BDE $(CH_{2\text{-oxirane}}) \sim 376$ kJ mol^{-1} in 2 methyl oxirane [32].

They indicate that $CH_{\alpha\text{-ether}}$ and $CH_{2\text{-oxirane}}$ sites are particularly oxidizable. It explains in part why kinetics for anhydrides build-up are faster for ELO + MHHPA 1–0.6 than ELO + MHHPA 1-1.

Let us now turn to the possible origins of the products absorbing at 1680 cm^{-1} (this wavenumber being actually the maxima of a broad peak). A mechanism can be based on the fact that the products are most formed in ELO + MHHPA 1-0.6 i.e. they must involve ether bridges and possibly residual oxiranes. Some possible mechanisms are given in Scheme 3. Despite other validation criteria are needed, it is interesting to notice that biacetyl groups display a shoulder in the 1650-1700 cm^{-1} [33] wavenumber range that could match with the observed changes.

(a)

(b)
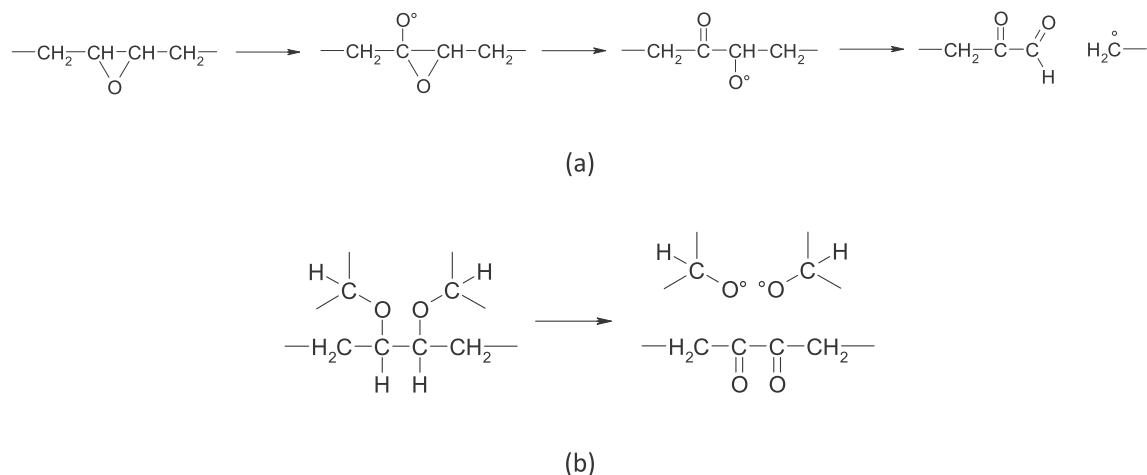
Scheme 3. Possible formation of biacetyl groups.
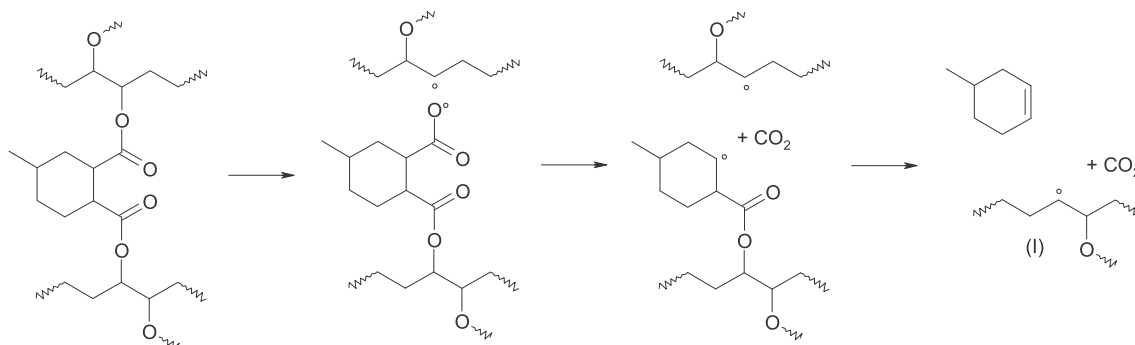
Scheme 4. Possible mechanism of formation of 4 methylcyclohexene (NB: scission of the second ester can maybe occurs just after the first decarboxylation).

In conclusion, the proposed mechanisms allow to explain in a certain extent why ELO + MHHPA 1-0.6 are more oxidizable (in terms of stable oxidation products) than ELO + MHHPA 1-1. Let us now try to explain why this second system exhibits a greater mass loss than its non-stoichiometric analogue.

4.2. On the effect of anhydride hardener on mass loss

Under nitrogen, the degradation of both ELO + MHHPA 1-1 and ELO + MHHPA 1-0.6 leads to the generation of 4-methylcyclohexene in very high quantity (almost 95% of the total weight loss). A possible mechanism of formation is based on the scission of the ester groups hold by the hardener followed by a decarboxylation (Scheme 4).

The fact that ELO + MHHPA 1-1 undergoes a very strong mass loss under nitrogen compared to ELO + MHHPA 1-0.6 can thus be explained as follows: in the stoichiometric compound, all epoxide rings were reacted with anhydride hardener so that some fatty acid chains can be strongly hindered by the presence of hardeners groups (in particular the linolenate ones). This results in spontaneous chain scissions (similarly with the unstable head to head isomers in PMMA) at high temperatures.

3 and 4-methylcyclohexanone are also observed for the decomposition under nitrogen. The fact they are in very low concentration compared to 4 methyl cyclohexene, and the presence of a ketone function hold by the cyclohexane ring suggests for us that this compound originates from the thermolysis of a hydroperoxide formed during the elaboration of the sample (Scheme 5).

The last compound observed in great quantity is the nonanal. A very simple mechanism can be proposed with the advantage of involving the (I) primary product (Schemes 4 and 5). In presence of oxygen, the secondary radical could react to give an ester group (and later an anhydride function) or can give a nonanal by a β-scission process (Scheme 6).

In conclusion, it seems that hardener group is associated to the strong level of mass loss: according to us, its presence induces a significant hindrance resulting in spontaneous decomposition (even in inert atmosphere). This one leads to methyl cyclohexene. Under air, the radicals oxidize and give supplementary VOC's. In any case, the concentration of MHHPA groups is higher in ELO + MHHPA 1-1 (Table 1) which explains why those networks are less stable in terms of mass loss. Interestingly, it is worth to be highlighted that thin samples display very high level of mass loss (Fig. 9) but remain relatively ductile. In other words, it suggests that the presence of several flexible group ensures a sufficient mobility (even at glassy state) to prevent cracking and keep a ductile behavior.

4.3. On the effect of anhydride hardener on the thickness of degraded layer

It was already established that the oxidized layer originates from the diffusion-reaction coupling for oxygen expressed by the following balance equation for oxygen:

$$\frac{\partial[O_2]}{\partial t} = D_{O2} \cdot \frac{\partial^2[O_2]}{\partial z^2} - r_{OX} \qquad (8)$$

where D_{O2} is the oxygen diffusivity and r_{OX} its consumption rate.

At steady state, the thickness of degraded layer can be approximated by [34]:
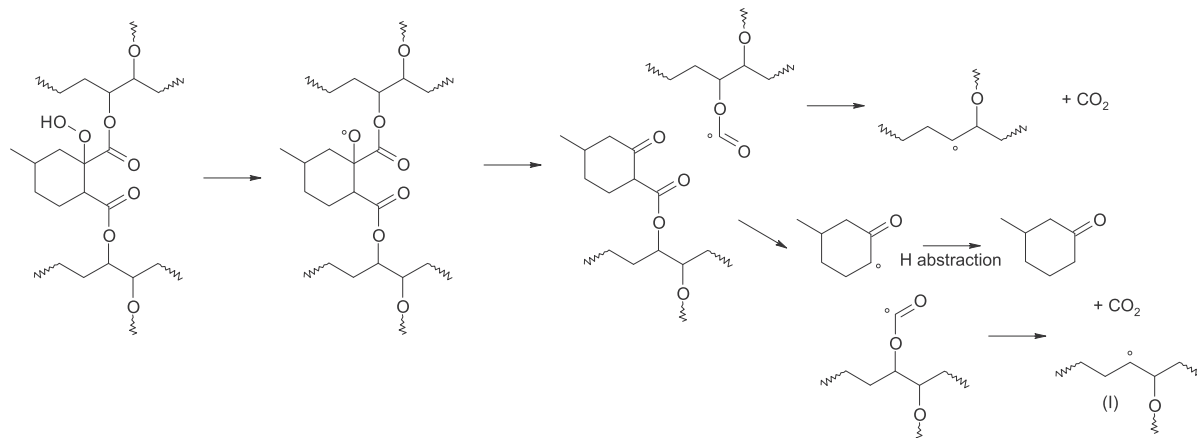
Scheme 5. Possible formation of 3 and 4 methyl cyclohexanone under nitrogen.

Scheme 6. Possible formation of nonanal.

$$TOL = \sqrt{\frac{D_{O2}\cdot[O_2]_S}{r_{OX}}} \tag{9}$$

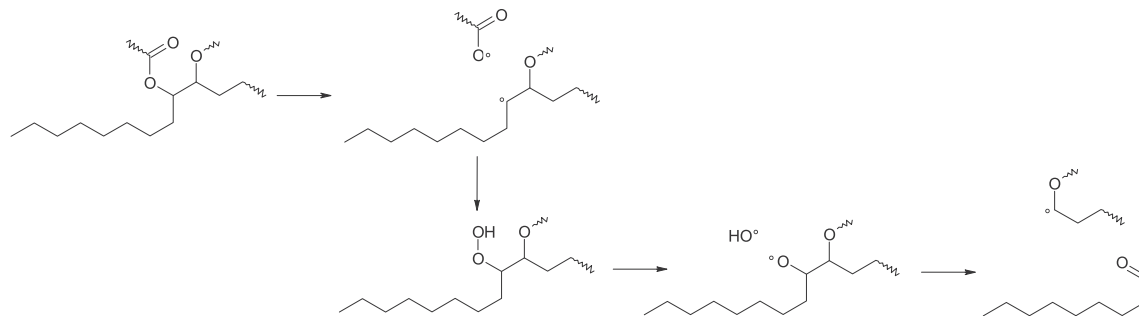As compared with microindentation, optical microscopy underestimates the thickness of the oxidized layer. Data are here clearly higher than previous observations in epoxy/amine systems characterized in similar conditions by optical, chemical [35] or mechanical changes [36].

Using Eq. (9), let us now try to reconcile the matter that:

- According to optical measurements (Fig. 12) and indentation measurements (Fig. 13):
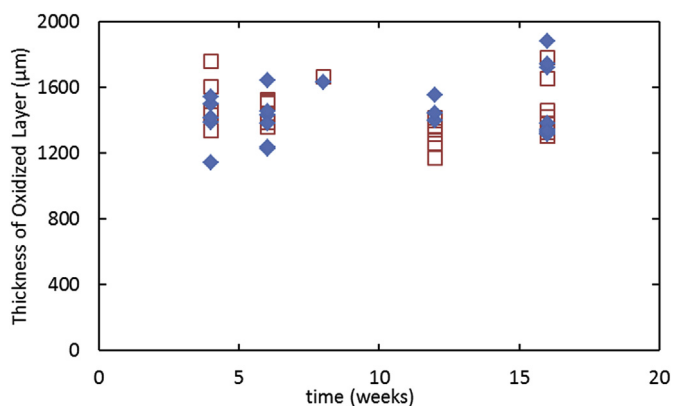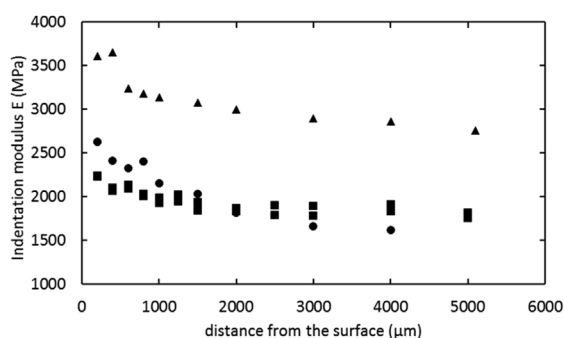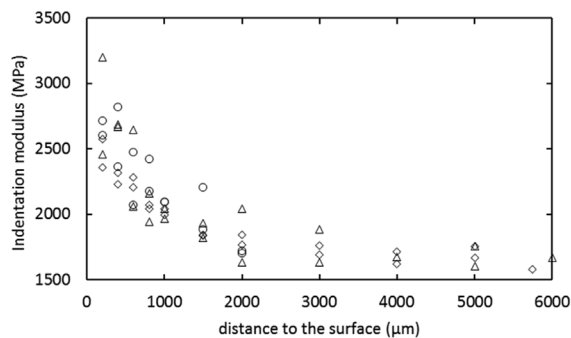
$(TOL)_{ELO+MHHPA\ 1-0.6} \geq (TOL)_{ELO+MHHPA\ 1-1}$

Fig. 12. Changes of thickness of Oxidized Layer estimated by optical microscopy for ELO + MHHPA 1-1 (◆) and 1−0.6 (□) aged at 160 °C.

- From the FTIR results (Figs. 6 and 7), it seems that (r_{OX})-$_{ELO+MHHPA\ 1-0.6} > (r_{OX})_{ELO+MHHPA\ 1-1}$

Results presented in Fig. 4 show than oxygen diffusivity and permeability is higher for ELO + MHHPA 1-0.6 than for ELO + MHHPA 1-1 in the 23−50 °C which might be interpreted in terms of free volume. If we consider now the value at higher temperatures (typically 160 °C which is the ageing temperature), two hypotheses can be considered [37]:

① There is no discontinuity at the glass transition. It is thus licit to extrapolate the data given in Fig. 4. The resulting oxygen permeability is hence expected to be higher in the non-stoichiometric system than in stoichiometric one. Basing on an Arrhenius extrapolation, diffusivity and permeability would be 15−20 and 5 times higher in ELO + MHHOPA 1-0.6 than in ELO + MHHPA 1-1.

② There is a discontinuity associated to free volume increase at T_g. According to Simha and Boyer [38], $\Delta\alpha.T_g$ is a constant at least in a reasonably restricted polymer family ($\Delta\alpha = \alpha_l - \alpha_g$ is the thermal expansion coefficient increase at T_g expressing the free volume increase). Since T_g is lower for non-stoichiometric networks than stoichiometric one (DMA analysis given in Appendix 3), $\Delta\alpha$ is higher for non-stoichiometric system and free volume quantity and the oxygen diffusivity as well.

Finally, it seems clear that in both cases, at 160 °C: $s_{O2}\times(D$-$_{O2})_{ELO+MHHPA\ 1-0.6}$ is slightly higher than $s_{O2}\times(D_{O2})_{ELO+MHHPA\ 1-1}$ which is well in line with the little difference in thickness of oxidized layers measurements in Figs. 11−12.

(a)

(b)

Fig. 13. Indentation profiles of ELO + MHHPA 1-1 (a) and 1-0-6 (b) thermally aged at 160 °C 4 (■,□), 8 (●,○) and 12 weeks (▲,△).

5. Conclusions

Non stoichiometric and stoichiometric epoxidized linseed oils (ELO) were cured with an anhydride hardener and thermally oxidized in the 120−200 °C temperature range, under air or elevated oxygen pressure. At molecular scale, the main oxidation product was anhydrides originating from the oxidation of C-H vicinal to esters and ethers located at the crosslink nodes. In non-stoichiometric systems with ELO excess, oxidation was observed to be faster which was explained from a higher concentration in reactive sites. However, in terms of consequences of oxidation, non-stoichiometric systems lead to a lower level of mass loss consistently with the matter that most of volatile byproducts generated by oxidation come from hardener. In the case of bulky materials, the thickness of oxidized layer seems slightly higher (at 160 °C at least) in non-stoichiometric systems than in stoichiometric one (despite mass loss are almost the same for bulky stoichiometric and non-stoichiometric systems). This was discussed from oxygen permeability measurements showing that the oxygen permeation in such systems is relatively high compared to other thermosets leading to possibly deep oxidized layer. In other words, this work offers an opportunity to design polymer matrices for thermosets with one biobased component by taking into account the effect of hardener triggering the cost, the initial properties, and long term stability.

Acknowledgements

Appendix 1

Appendix 2

Let us for example consider the following mechanism for describing the chemical changes in the network:
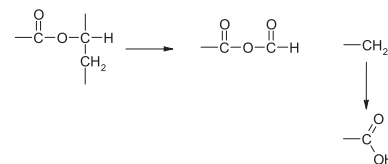
It is documented that glassy elastic modulus is correlated with the density of cohesive energy [42]:

$$E_0 = 3.K_0.(1-2\upsilon)$$

Where E_0, K_0 and υ are respectively the elastic and compressive moduli and the Poisson's ratio.

The compressive modulus (or Bulk Modulus) is thus given by Ref. [42]:

$$K_0 \sim 11.CED \sim 11.E_{coh}/V_m$$

Where E_{coh} is the cohesive energy (J mol^{-1}), V_m is the molar volume (cm^3 mol^{-1}) and CED is the density of cohesive energy (MPa$^{1/2}$).

E_{coh} and V_m can be calculated according to the incremental method based on additive group contribution proposed by Van Krevelen [43] (Table 4):

Table 3
Permeability P (in cm^3 cm cm^{-2} s^{-1} Pa^{-1}) and diffusivity D (in cm^2 s^{-1}) in some thermoset polymers [24,37,39–41].

	Main componants (%)	T (°C)	10^{15}.P	10^8.D	ref
Polyester	UP resin (25%)	23	1.0	0.57	[39]
	Limestone (52.7%)	40	2.2	1.26	
	Short GF (15)	60	5.2	2.77	
polyester	UP resin (26)	23	3.1	1.03	[39]
	Limestone (26)	40	7.0	2.80	
	China clay (38.3)	60	17.0	8.00	
Polyester	UP resin (100)	25	0.7	3.60	[24]
		100	2.3	19.50	
Polyester	UP resin (32)	25	0.3	2.30	[24]
	ATH + Zn Borate (68)	100	2.4	13.30	
Epoxy	DGEBA + PGE + DDM	30	9.8	0.24	[40]
		40	19.3	0.28	
Epoxy	DGEBA + DDM	10	2.3	0.15	[40]
		20	3.3	0.16	
		30	7.6	0.16	
Epoxy	DEGBA + 4,4′-methylenebis(2-methylcyclohexylamine)	25	10.6	0.50	[37]
		40	18.2	1.01	
		50	25.1	1.67	
Epoxy	DGEBA + jeffamine 230	25	5.7	0.29	[37]
		40	9.7	0.58	
		50	12.3	1.17	
Epoxy	ELO + MHHPA 1-1	23	59.1	4.45	this work
		40	109.3	5.45	
		50	158.3	6.47	
Epoxy	ELO + MHHPA 1-0.6	23	83.7	6.05	this work
		40	199.0	11.50	
		50	301.6	17.30	
PDCPD		23	197.5	7.90	[41]
		35	293.7	9.18	
		40	293.7	10.20	
		50	62.8	12.10	

Table 4
Additive group contribution for cohesive energy.

Group	E_{coh} (J mol^{-1})	V_m (cm^3 mol^{-1})
Anhydride	30560	30
Ester	18000	18
-COOH	27630	28.5
CH$_2$	4940	16.1
CH	3430	-1

One sees that E_{coh} increases from about 800 to about 1000 MPa which justifies the glassy moduli increase.
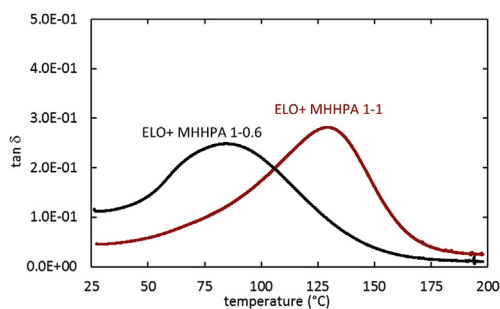
Appendix 3

Fig. 14. T_g determination from DMA analysis in flexural mode (2 °C min^{-1}, 1 Hz, 0.1%).

References

[1] J.S. Siracusa, L. Yin, E. Measel, S. Liang, X. Yu, Effects of bisphenol A and its analogs on reproductive health: a mini review, Reprod. Toxicol. 79 (2018) 96−123.

[2] E.L.M. Vermeirssen, C. Dietschweiler, I. Werner, M. Burkhardt, Corrosion protection products as a source of bisphenol A and toxicity to the aquatic environment, Water Res. 123 (2017) 586−593.

[3] M.F. Kanz, L. Kaphalia, B.S. Kaphalia, E. Romagnoli, G.A.S. Ansari, Methylene dianiline: acute toxicity and effects on biliary function, Toxicol. Appl. Pharmacol. 117 (1) (1992) 88−97.

[4] G.P. Carlson, Modification of the metabolism and toxicity of styrene and styrene oxide in hepatic cytochrome P450 reductase deficient mice and CYP2F2 deficient mice, Toxicology 294 (2−3) (2012) 104−108.

[5] M. Kogevinas, G. Ferro, A. Andersen, T. Bellander, M. Biocca, D. Coggon, V. Gennaro, S. Hutchings, H. Kolstad, I. Lundberg, E. Lynge, T. Partanen, R. Saracci, Cancer mortality in a historical cohort study of workers exposed to styrene, Scand. J. Work. Environ. Health 20 (4) (1994) 251−261.

[6] Y.-D. Li, X.-Y. Jian, J. Zhu, A.-K. Du, J.-B. Zeng, Fully biobased and high performance epoxy thermosets from epoxidized soybean oil and diamino terminated polyamide 1010 oligomers, Polym. Test. 72 (2018) 140−146.

[7] R.-T. Zeng, Y. Wu, Y.-D. Li, M. Wang, J.-B. Zeng, Curing behavior of epoxidized soybean oil with biobased dicarboxylic acids, Polym. Test. 57 (2017) 281−287.

[8] N. Boquillon, C. Fringant, Polymer networks derived from curing of epoxidised linseed oil: influence of different catalysts and anhydride hardeners, Polymer 41 (24) (2000) 8603−8613.

[9] Y. Chen, Z. Xi, L. Zhao, New bio-based polymeric thermosets synthesized by ring-opening polymerization of epoxidized soybean oil with a green curing agent, Eur. Polym. J. 84 (2016) 435−447.

[10] A. Dupuis, F.-X. Perrin, A. Ulloa Torres, J.-P. Habas, L. Belec, J.-F. Chailan, Photo-oxidative degradation behavior of linseed oil based epoxy resin, Polym. Degrad. Stabil. 135 (2017) 73−84.

[11] Y. Chen, Z. Xi, L. Zhao, New bio-based polymeric thermosets synthesized by ring-opening polymerization of epoxidized soybean oil with a green curing agent, Eur. Polym. J. 84 (2016) 435−447.

[12] A. Demirbas, Production of biodiesel fuels from linseed oil using methanol and ethanol in non-catalytic SCF conditions, Biomass Bioenergy 33 (1) (2009) 113−118.

[13] A. Raj Mahendran, G. Wuzella, A. Kandelbauer, N. Aust, Thermal cure kinetics of epoxidized linseed oil with anhydride hardener, J. Therm. Anal. Calorim. 107 (2012) 989−998.

[14] L. Matějka, J. Lövy, S. Pokorný, K. Bouchal, K. Dušek, Curing epoxy resins with anhydrides. Model reactions and reaction mechanism, J. Polym. Sci. Polym.

Chem. Ed. 21 (10) (1983) 2873−2885.

[15] M.F. Doener, W.D. Nix, A method for interpreting the data from depth sensing indentation instruments, J. Mater. Res. 1 (1986) 601−609.

[16] Metallic Materials – Instrumented Indentation Test for Hardness and Materials Parameters – Part 1: Test Method. ISO/DIS Standard 14577-1:2002.

[17] W.C. Oliver, G.M. Pharr, An improved technique for determining hardness and elastic modulus using load and displacement sensing indentation experiments, J. Mater. Res. 7 (6) (1992) 1564−1583.

[18] J. Crank, The Mathematics of Diffusion, second ed., Clarenson Press, Oxford, 1975, pp. 44−68. Chap. 4. Diffusion in a plane sheet.

[19] A. Guinault, C. Sollogoub, V. Ducruet, S. Domenek, Impact of crystallinity of poly (lactide) on helium and oxygen barrier properties, Eur. Polym. J. 48 (2012) 779−788.

[20] Interpreting Infrared, Raman, and Nuclear Magnetic Resonance Spectra, vol. 1, 2001, pp. 205−212.

[21] X. Gu, C.Q. Yang, FT-IR and FT-Raman spectroscopy study of the cyclic anhydride intermediates for esterification of cellulose: I. Formation of anhydrides without a catalyst, Res. Chem. Intermed. 24 (9) (1998) 979−996.

[22] L.J. Bellamy, B.R. Connelly, A.R. Philpotts, R.L. Williams, The infrared spectra of anhydrides and peroxides, Ber. Bunsen Ges. Phys. Chem. 64 (5) (1960) 563−566.

[23] X. Colin, J. Verdu, Strategy for studying thermal oxidation of organic matrix composites, Compos. Sci. Technol. 65 (3−4) (2005) 411−419.

[24] J.S. Arrieta, E. Richaud, B. Fayolle, F. Nizeyimana, Thermal oxidation of vinyl ester and unsaturated polyester resins, Polym. Degrad. Stabil. 129 (2016) 142−155.

[25] M. Minervino, M. Gigliotti, M.C. Lafarie-Frenot, J.C. Grandidier, The effect of thermo-oxidation on the mechanical behaviour of polymer epoxy materials, Polym. Test. 32 (6) (2013) 1020−1028.

[26] S. Terekhina, M. Mille, B. Fayolle, X. Colin, Oxidation induced changes in viscoelastic properties of a thermostable epoxy matrix, Polym. Sci. 55 (10) (2013) 614−624.

[27] M. Celina, J. Wise, D.K. Ottesen, K.T. Gillen, R.L. Clough, Oxidation profiles of thermally aged nitrile rubber, Polym. Degrad. Stabil. 60 (2−3) (1998) 493−504.

[28] M. Ochi, H. Iesako, M. Shimbo, Relaxation mechanism of epoxide resin cured with acid anhydrides. III. Effect of alkyl side chains on mechanical and dielectric β relaxations, J. Polym. Sci. B Polym. Phys. 24 (6) (1986) 1271−1282.

[29] S. Michaille, P. Arlaud, J. Lemaire, Photolyse et photo-oxydation de polyesters insatures—2. Comportement du polymaleate-isophtalate de propylene glycol reticule ou non, Eur. Polym. J. 29 (1) (1993) 35−46.

[30] V. Saheb, S. Mohammad, A. Hosseini, Theoretical studies on the kinetics and mechanism of multi-channel gas-phase unimolecular reaction of ethyl acetate, Computational and Theoretical Chemistry 1009 (2013) 43−49.

[31] B. Akih-Kumgeh, J.M. Bergthorson, Structure-reactivity trends of C1−C4 alkanoic acid methyl esters, Combust. Flame 158 (6) (2011) 1037−1048.

[32] E.T. Denisov, I.B. Afanas'ev, Oxidation and Antioxidants in Organic Chemistry and Biology, Taylor & Francis, Boca Raton, FL, 2005. Oxidation of Alcohols and Ethers. Table 7.11.

[33] https://webbook.nist.gov/cgi/cbook.cgi?ID=C431038&Type=IR-SPEC&Index=1#IR-SPEC.

[34] L. Audouin, V. Langlois, J. Verdu, J.C.M. de Bruijn, Role of oxygen diffusion in polymer ageing: kinetic and mechanical aspects, J. Mater. Sci. 29 (3) (1994) 569−583.

[35] X. Colin, C. Marais, J. Verdu, A new method for predicting the thermal oxidation of thermoset matrices: application to an amine crosslinked epoxy, Polym. Test. 20 (7) (2001) 795−803.

[36] M. Pecora, Y. Pannier, M.-C. Lafarie-Frenot, M. Gigliotti, C. Guigon, Effect of thermo-oxidation on the failure properties of an epoxy resin, Polym. Test. 52 (2016) 209−217.

[37] M.C. Celina, A. Quintana, Oxygen diffusivity and permeation through polymers at elevated temperature, Polymer 150 (2018) 326−342.

[38] R. Simha R.F. Boyer, On a general relation involving the glass temperature and coefficients of expansion of polymers, J. Chem. Phys. 37 (5) (1962) 1003−1007.

[39] S. Pauly, The radiation resistance of thermoset plastics—III. Oxygen permeation experiments, Int. J. Radiat. Appl. Instrum. C Radiat. Phys. Chem. 39 (3) (1992) 269−272.

[40] C. Damian, E. Espuche, M. Escoubes, Influence of three ageing types (thermal oxidation, radiochemical and hydrolytic ageing) on the structure and gas transport properties of epoxy−amine networks, Polym. Degrad. Stabil. 72 (3) (2001) 447−458.

[41] V. Defauchy, P.Y. Le Gac, A. Guinault, J. Verdu, G. Recher, R. Drozdzak, E. Richaud, Kinetic analysis of polydicyclopentadiene oxidation, Polym. Degrad. Stabil. 142 (2017) 169−177.

[42] J.-P. Pascault, H. Sauterau, J. Verdu, R.J.J. Williams, Thermosetting Polymers, Marcel Dekker, 2002. Chap 10. Basic Physical Properties of Networks.

[43] D.W. Van Krevelen, K. Te Nijenhuis, Properties of Polymers – Their Correlation with Chemical Structure; Their Numerical Estimations and Prediction from Additive Group Contributions. Fourth, Completely Revised Edition, Elsevier, Amsterdam, 2009. Chap. 6.